ELASTODYNAMIC OPTICAL THEOREM FOR THE EVALUATION OF SCATTERING CROSS-SECTIONS FOR A CRACK

M. Kitahara
School of Marine Science and Technology
Tokai University, Shimizu, Shizuoka 424, Japan

K. Nakagawa
UNITEC
Kawasaki-ku, Kawasaki, Kanagawa 210, Japan

INTRODUCTION

Scattering cross-sections are calculated for a crack in three-dimensional elastic solids. The crack opening displacements are evaluated first by the boundary element methods. Then the scattering amplitudes for the crack are derived from the far-field representations of the scattered fields. In the final step to calculate the scattering cross-sections from scattering amplitudes, two methods are compared. One is the method based on the definition and here the scattering cross-section is calculated from the integration of the differential cross-sections over the solid angle. The other is the method based on the elastodynamic counterpart of the optical theorem. It is verified that the results obtained from the elastodynamic optical theorem are accurate enough to evaluate the scattering cross-section for the crack in elastic solids.

The elastodynamic optical theorem has been derived for an arbitrary shaped scatterer in elastic solids[1,2]. For NDE applications, the elastodynamic counterpart of the optical theorem is a useful tool to evaluate the total scattering cross-section which relates to the ultrasonic attenuation of the inhomogeneous materials[3,4]. The total scattering cross-sections have been calculated for a penny-shaped crack by semi-analytical methods[5,6]. For the three-dimensional solid, the boundary element methods have been developed for the dynamic crack problems[7,8] and an application has been shown for the evaluation of the total scattering cross-section[8]. The combination of the boundary element method and the elastodynamic optical theorem has advantages of the applicability to the arbitrary shaped crack and the effectiveness to calculate the total scattering cross-section.

CRACK OPENING DISPLACEMENT

The method to determine the crack opening displacement is summarized first, because the accuracy of the crack opening displacement for a given incident wave

Review of Progress in Quantitative Nondestructive Evaluation, Vol 16
Edited by D.O. Thompson and D.E. Chimenti, Plenum Press, New York, 1997

field affects the final results of the cross-sections. For the planar crack S_C shown in Figure 1, the x_2 axis of the coordinate is chosen so as to coincide with the unit normal vector for the crack surface, with no loss of generality. Then the scattered wave field u_k^{SC} is expressed as

$$u_k^{SC}(\mathbf{x}) = \int_{S_C} \Xi_{km2}(\mathbf{x},\mathbf{y})\Delta u_m(\mathbf{y})dS_y \ , \qquad \mathbf{x} \in D \tag{1}$$

where Δu_m is the crack opening displacements and Ξ_{kmn} is the stress Green's function for the full-space. The operation $C_{ijkl}\partial/\partial x_l$ leads to the following stress components

$$\sigma_{2j}^{SC}(\mathbf{x}) = C_{2jkl}\int_{S_C} \Xi_{km2,l}(\mathbf{x},\mathbf{y})\Delta u_m(\mathbf{y})dS_y \ , \qquad \mathbf{x} \in D \ . \tag{2}$$

The integral kernel of the above expression becomes hyper-singular when the field point $\mathbf{x}$ approaches to the crack surface, because of the derivative of the stress Green's function. In order to reduce the singularity, the stress Green's function Ξ_{kmn} is divided into the sum of the singular term Ξ_{kmn}^0 and the regular term $\sum \Xi_{kmn}^n$

$$\Xi_{kmn} = \Xi_{kmn}^0 + \sum_n \Xi_{kmn}^n \tag{3}$$

where the term Ξ_{kmn}^0 is the first term of the Taylor expansion of the stress Green's function and the term Ξ_{kmn}^n is the remaining terms of $n(=1,2,3\cdots)$. Here, the term Ξ_{kmn}^0 coincides with the stress Green's function in elastostatics. Then the expression in Equation (2) reduces to

$$\begin{aligned}\sigma_{2j}^{SC}(\mathbf{x}) = &\int_{S_C} C_{2jk\alpha}\Xi_{km2,\alpha}^0\Delta u_m(\mathbf{y})dS_y + \sum_n \int_{S_C} C_{2jk\alpha}\Xi_{km2,\alpha}^n\Delta u_m(\mathbf{y})dS_y \\ &+ \int_{S_C} C_{2jk2}\Xi_{km2,2}^0\Delta u_m(\mathbf{y})dS_y + \sum_n \int_{S_C} C_{2jk2}\Xi_{km2,2}^n\Delta u_m(\mathbf{y})dS_y \end{aligned} \tag{4}$$

where $\alpha = 1,3$ are components along the crack surface and the differentiation $(\cdot)_{,\alpha}$ is on the field point $\mathbf{x}$. The hyper-singularity arises from the first and third terms in Equation (4). The integration by parts is introduced for the first term, and the equilibrium condition $\Xi_{km2,2}^0 = -\Xi_{km\alpha,\alpha}^0$ and the integration by parts are used for the third term. The result is

$$\begin{aligned}\sigma_{2j}^{SC}(\mathbf{x}) = &\int_{S_C} C_{2jk\alpha}\Xi_{km2}^0\Delta u_{m,\alpha}(\mathbf{y})dS_y + \sum_n \int_{S_C} C_{2jk\alpha}\Xi_{km2,\alpha}^n\Delta u_m(\mathbf{y})dS_y \\ &- \int_{S_C} C_{2jk2}\Xi_{km\alpha}^0\Delta u_{m,\alpha}(\mathbf{y})dS_y + \sum_n \int_{S_C} C_{2jk2}\Xi_{km2,2}^n\Delta u_m(\mathbf{y})dS_y \end{aligned} \tag{5}$$

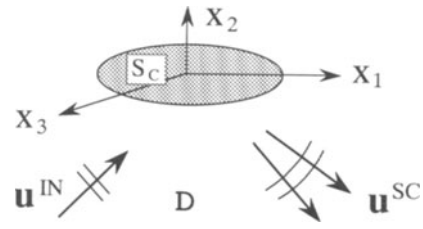

Figure 1. Crack S_C in three-dimensional elastic space D.

where the differentiation of $\Delta u_{m,\alpha}(\mathbf{y})$ is on the source point $\mathbf{y}$. The limit to the boundary $\mathbf{x} \in D \rightarrow \mathbf{x} \in S_C$ is taken in the stage of the expression of Equation (5).

From the boundary condition on the surface of the crack

$$\sigma_{2j}^{SC}(\mathbf{x}) = -\sigma_{2j}^{IN}(\mathbf{x}) \ , \qquad \mathbf{x} \in S_C \tag{6}$$

where $\sigma_{2j}^{IN}(\mathbf{x})$ is the stress induced by the incident wave, the boundary integral equation to determine the crack opening displacement Δu_m can be obtained. The boundary integral equation is solved by the boundary element method. The quadratic elements with 8 nodes are introduced to approximate the crack opening displacements and the quarter point elements are used as the crack tip elements.

SCATTERING AMPLITUDE

Introduction of the far-field approximation to the Green's function in Equation (1) leads to the far-field expression of the scattered wave

$$u_i^{SC}(\mathbf{x}) = \int_{S_C} \hat{\Xi}_{ijk}(\mathbf{x}, \mathbf{y}) n_k \Delta u_j(\mathbf{y}) dS_y \tag{7}$$

where $\mathbf{n} = (0, 1, 0)$ is the unit normal vector of the crack surface. The $\hat{\Xi}_{ijk}$ is the far-field expression of the stress Green's function and has the form

$$\hat{\Xi}_{ijk} = \sum_{\alpha=L,T,H} \Xi_{ijk}^{\alpha} \tag{8}$$

where the summation is taken for the longitudinal ($\alpha = L$) and transverse ($\alpha = T, H$) wave components. Each term Ξ_{ijk}^{α} can be obtained from the stress derivative

$$\Xi_{ijk}^{\alpha} = C_{jkml} \frac{\partial U_{im}^{\alpha}}{\partial y_l} = -ik_\alpha C_{jkml} \hat{x}_l U_{im}^{\alpha} \ . \tag{9}$$

In Equation (9), U_{im}^{α} is the $\alpha(= L, T, H)$ wave component in the far-field expression of the displacement Green's function for the point force and has the form

$$U_{ij}^{\alpha} = \frac{\exp(ik_\alpha x)}{4\pi\rho c_\alpha^2 x} \exp(-ik_\alpha \hat{\mathbf{x}} \cdot \mathbf{y}) f_i^{\alpha} f_j^{\alpha} \tag{10}$$

where $\hat{\mathbf{x}}$ is the unit vector points to the far-field point $\mathbf{x}$ from the origin of the coordinate, $x = |\mathbf{x}|$, and f_i^{α} is the polarization vector of the $\alpha(= L, T, H)$ wave component as shown in Figure 2.

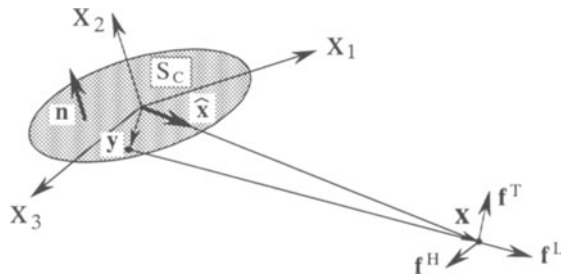

Figure 2. Far-field point $\mathbf{x}$ and unit vector $\hat{\mathbf{x}}$.

From Equations (8)∼(10), the scattered far-field u_i^{SC} can be rewritten as

$$u_i^{SC}(\mathbf{x}) = \sum_{\alpha=L,T,H} A_i^\alpha \frac{\exp(ik_\alpha x)}{x} \tag{11}$$

where A_i^α is the scattering amplitude of the longitudinal ($\alpha = L$) and transverse ($\alpha = T, H$) wave components and it has the form

$$A_i^\alpha = ik_\alpha f_i^\alpha f_n^\alpha I_n^\alpha(\hat{\mathbf{x}}) \ . \tag{12}$$

The term $I_n^\alpha(\cdot)$ is the integration of the crack opening displacements over the crack surface in the following sense

$$I_n^\alpha(\hat{\mathbf{x}}) = -\frac{C_{kjnl}\hat{x}_l}{4\pi\rho c_\alpha^2} \int_{S_C} n_k(\mathbf{y}) \Delta u_j(\mathbf{y}) e^{-\imath k_\alpha \hat{\mathbf{x}}\cdot\mathbf{y}} dS_y \ . \tag{13}$$

The stress component $\sigma_{ij}^{SC}(\mathbf{x}) = C_{ijkl}\partial u_k^{SC}(\mathbf{x})/\partial x_l$ in the far-field is obtained from Equation (11) as

$$\sigma_{ij}^{SC}(\mathbf{x}) = \sum_{\alpha=L,T,H} B_{ij}^\alpha \frac{\exp(ik_\alpha x)}{x} \tag{14}$$

where the stress amplitude B_{ij}^α can be calculated by the scattering amplitude A_i^α

$$B_{ij}^\alpha(\mathbf{x}) = ik_\alpha\{\lambda\delta_{ij}\hat{x}_k A_k^\alpha + \mu(\hat{x}_i A_j^\alpha + \hat{x}_j A_i^\alpha)\} \ . \tag{15}$$

SCATTERING CROSS-SECTIONS

Evaluation Based on Definition

The total scattering cross-section P is defined as the ratio of the scattered power to the intensity of the incident wave. It is convenient to evaluate the differential cross-section $dP/d\Omega$ first

$$\frac{dP(\omega)}{d\Omega} = \lim_{x\to\infty} -\frac{\omega}{2} \frac{Im[x^2\hat{x}_i\sigma_{ij}^{SC}(\mathbf{x},\omega)u_j^{SC*}(\mathbf{x},\omega)]}{< I >} \tag{16}$$

where $d(\cdot)/d\Omega$ is the differentiation with respect to the solid angle, u_j^{SC*} is the complex conjugate of the scattered field u_j^{SC}, and ω is the angular frequency.

For the plane longitudinal incident wave with the unit amplitude

$$u_i^{IN} = p_i \exp(ik_L \mathbf{p}\cdot\mathbf{x}), \qquad (|\mathbf{p}| = 1) \tag{17}$$

the time averaged intensity of the incident wave $< I >$ in Equation (16) reduces to

$$< I >= -\frac{1}{2}\omega k_L(\lambda + 2\mu) \ . \tag{18}$$

Equations (16) and (17) lead to the expression

$$\frac{dP(\omega)}{d\Omega} = \lim_{x\to\infty} \frac{x^2 Im(\hat{x}_i \sigma_{ij}^{SC} u_j^{SC*})}{k_L(\lambda + 2\mu)} \ . \tag{19}$$

The displacement u_j^{SC} and stress σ_{ij}^{SC} in the far-field are given in Equations (11) and (14). Introduction of Equations (11) and (14) to Equation (19) leads to the following expression for the differential cross-section

$$\frac{dP}{d\Omega} = |\mathbf{A}^L|^2 + \frac{k_L}{k_T}(|\mathbf{A}^T|^2 + |\mathbf{A}^H|^2) \tag{20}$$

where $\mathbf{A}^\alpha$ is the scattering amplitude in Equations (12) and (13) for the α-wave component.

The total scattering cross-section can be obtained from the integration of the differential scattering cross-section with respect to the solid angle on the unit sphere

$$P(\omega) = \iint \frac{dP}{d\Omega} \sin\theta d\theta d\phi \ . \tag{21}$$

In this method, the scattering amplitude is calculated from Equations (12) and (13) and then the differential cross-section is evaluated from Equation (20). The final integration in Equation (21) can be carried out numerically. The Gaussian quadrature formula is adopted in the examples of this paper.

Elastodynamic Optical Theorem

In the elastodynamic optical theorem, the total scattering cross-section can be evaluated from the scattering amplitudes in the forward direction[1,2]. For the incident longitudinal wave given in Equation (17), the elastodynamic optical theorem can be written in the form

$$P(\omega) = \frac{4\pi}{k_L} Im[\mathbf{p} \cdot \mathbf{A}^L(\mathbf{p})] \tag{22}$$

where $\mathbf{A}^L$ is the vector of the longitudinal scattering amplitude and $\mathbf{A}^L$ is estimated in the forward $\mathbf{p}$ direction, here $\mathbf{p}$ is the unit propagation vector of the incident longitudinal wave in Equation (17). In this case, the scattering amplitude is calculated from Equations (12) and (13) in the forward direction and the total scattering cross-section is directly obtained from Equation (22).

NUMERICAL EXAMPLES

The circular crack with radius a has been chosen as an example. In the calculation of the crack opening displacements, the quadratic isoparametric elements have been adopted, here the surface of the crack has been divided into 60 elements with total 181 nodes. The crack opening displacements calculated at nodes have been used for the evaluation of scattering amplitudes.

Calculation Based on Definition

In the calculation of the scattering cross-sections, the method based on the definition has an advantage to understand the general feature of the distribution

for the scattered power of L, T, and H wave components for the crack. Figure 3 shows the distribution of the differential cross-sections in the $x_1 - x_2$ plane. The incident wave is the plane longitudinal wave with the propagation direction $\mathbf{p} = (\sin\theta^I, \cos\theta^I, 0)$ and $\theta^I = 30°$. The Poisson's ratio of the elastic matrix is $\nu = 1/4$. Figures (a), (b), and (c) show the scattered power patterns for the nondimensional wave numbers ak_T=1.0, 2.0, and 3.0, respectively. In the figures, the differential cross-section $dP/d\Omega(= |\mathbf{A}^L|^2 + (k_L/k_T)(|\mathbf{A}^T|^2 + |\mathbf{A}^H|^2)$ is denoted by black circles, the longitudinal component $|\mathbf{A}^L|^2$ by white circles, and the transverse component $(k_L/k_T)|\mathbf{A}^T|^2$ by white squares. The other transverse component $(k_L/k_T)|\mathbf{A}^H|^2$ is very small in this $x_1 - x_2$ plane. The coefficient k_L/k_T is $1/\sqrt{3}$ for the Poisson's ratio $\nu = 1/4$. Figure 4 shows the normalized total scattering cross-section $P/\pi a^2$ for the normalized wavenumber ak_T. The incident wave is the same longitudinal wave with Figure 3. The results by Krenk and Schmidt[5] are shown in white squares.

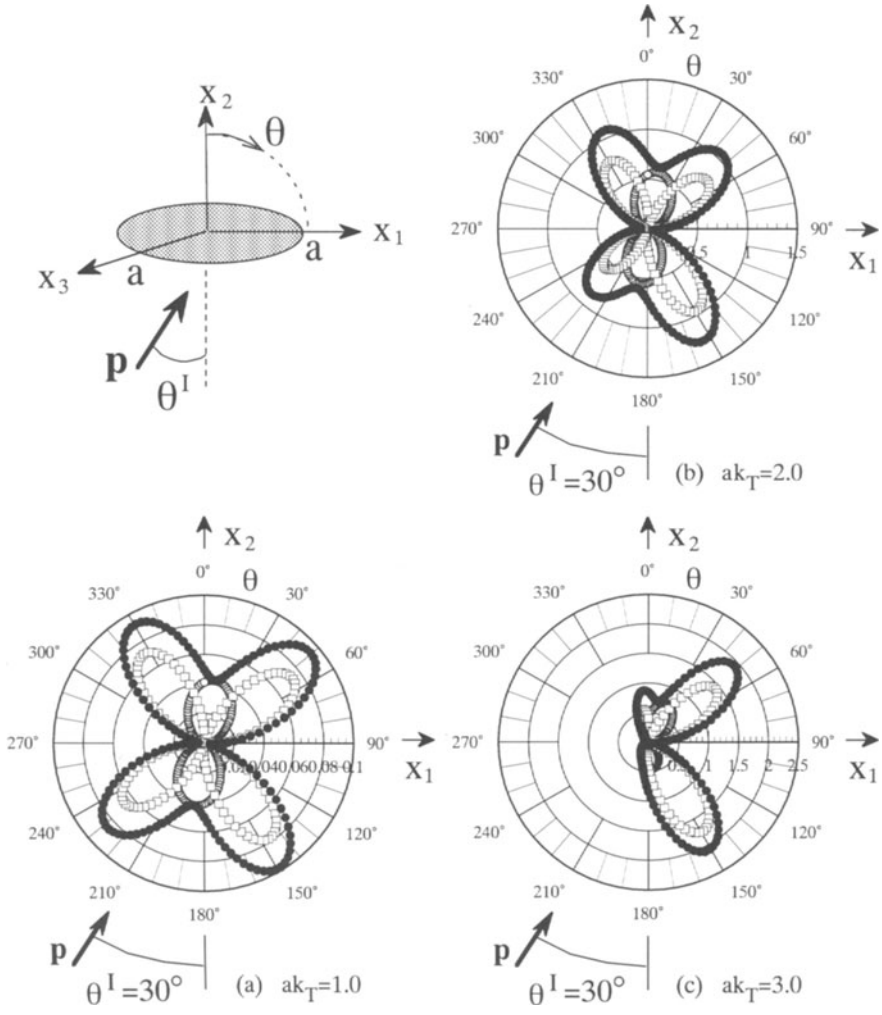

Figure 3. Differential cross-sections $dP/d\Omega$ in $x_1 - x_2$ plane for longitudinal wave incidence with propagation vector $\mathbf{p} = (\sin\theta^I, \cos\theta^I, 0)$; Black circles are $dP/d\Omega(= |\mathbf{A}^L|^2 + (k_L/k_T)(|\mathbf{A}^T|^2 + |\mathbf{A}^H|^2)$, white circles are $|\mathbf{A}^L|^2$, white squares are $(k_L/k_T)|\mathbf{A}^T|^2$, and components $(k_L/k_T)|\mathbf{A}^H|^2$ are very small in this case.

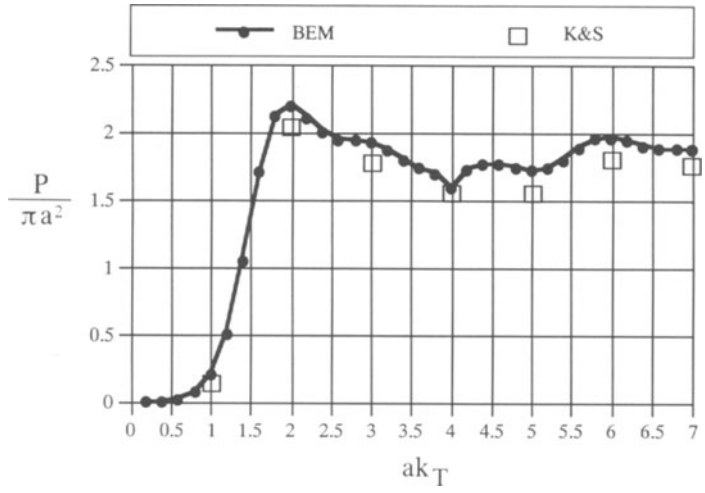

Figure 4. Normalized total scattering cross-section $P/\pi a^2$ for longitudinal wave incidence with $\theta^I = 30°$.

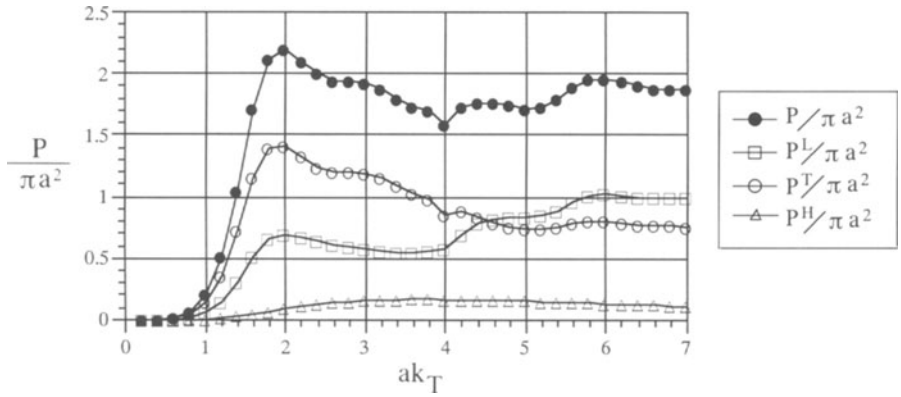

Figure 5. Contribution of longitudinal($P^L/\pi a^2$) and transverse components ($P^T/\pi a^2$, $P^H/\pi a^2$) to the total cross-section($P/\pi a^2$).

Figure 5 explains the contribution of the longitudinal and transverse components of the scattered power to the total cross-section. The longitudinal component $P^L/\pi a^2$ is denoted by white squares, the transverse components $P^T/\pi a^2$ and $P^H/\pi a^2$ by white circles and white triangles, respectively.

Total cross – section by Elastodynamic Optical Theorem

The optical theorem has an advantage to evaluate the total scattering cross-sections directly from the scattering amplitudes in the forward direction. In the three-dimensional numerical calculations, this advantage becomes important because of the saving of the computer memory and time. Table 1 shows the comparison of total scattering cross-sections calculated by the method based on the definition in Equation (21) and by the optical theorem in Equation (22). The incident wave is the same longitudinal wave as in Figure 3. The incident angle is $\theta^I = 30°$.

Table 1. Total scattering cross-sections calculated by the method based on the definition and by the optical theorem.

$\theta^I = 30°$

ak_T	$P/\pi a^2$		ak_T	$P/\pi a^2$	
	Def.	Optical Th.		Def.	Optical Th.
1.0	0.204	0.204	4.0	1.588	1.665
2.0	2.195	2.188	5.0	1.721	1.699
3.0	1.922	1.906	6.0	1.959	1.946

For all values of ak_T=1, 2, 3, 4, 5, and 6, the total cross-sections evaluated from the optical theorem have quite good agreement with the values calculated by the method based on the definition. It is interesting to note the scattered power patterns in Figure 3. Here, the scattered powers are not only in the forward direction, rather in the specular direction. Furthermore, it is to be noted that the power of the scattered transverse wave components is not weak from Figures 3 and 5. Finally, from the results in Table 1, it is concluded that the optical theorem is the effective tool to evaluate the total scattering cross-sections for the crack.

REFFRENCES

1. P.J. Barratt and W.D. Collins, Proc. Camb. Phil. Soc. 61, 969(1965).
2. J.E. Gubernatis, E. Domany and J.A. Krumhansl, J. Appl. Phys. 48, 2804 (1977).
3. A.I. Beltzer, Wave Motion 11, 211(1989).
4. S.M. Nair, D.K. Hsu and J.H. Rose, J. Nondestructive Evaluation 8, 13(1989).
5. S. Krenk and H. Schmidt, Phil. Trans. R. Soc. Lond. A308, 167(1982).
6. P.A. Martin and G.W. Wickham, Proc. R. Soc. Lond. A390, 91(1983).
7. N. Nishimura and S. Kobayashi, in *Advanced Boundary Element Methods*, ed. T.A. Cruse(Springer-Verlag, Berlin Heidelberg, 1988), p.279.
8. D.E. Budreck and J.D. Achenbach, J. Appl. Mech. 55, 405(1988).